Nonpolar Resistive Switching in Ag@TiO_2 Core-Shell Nanowires.

Hugh G. Manning[†, §], *Subhajit Biswas*[§, ϕ], *Justin D. Holmes* [§, ϕ], *John J. Boland* [†, §, *]

[†] School of Chemistry, Trinity College Dublin, Dublin 2, Ireland

[§]Center for Research on Adaptive Nanostructures and Nanodevices (CRANN) & Advanced Materials and Bioengineering Research (AMBER) Research Center, Trinity College Dublin, Dublin 2, Ireland.

[ϕ] School of Chemistry, University College Cork, Cork, Ireland

Keywords: silver, titanium dioxide, core-shell, nanowire, nonpolar resistive switching

ABSTRACT: Nonpolar resistive switching, a combination of bipolar and unipolar resistive switching, is demonstrated for the first time in a single nanowire system. Exploiting Ag@TiO_2 core-shell nanowires synthesized by post-growth shell formation the switching mode is controlled by adjusting the current compliance effectively tailoring the electrical polarity response. We demonstrate ON/OFF ratios of 10^5 and 10^7 for bipolar and unipolar modes respectively. In the bipolar regime, retention times could be controlled up to 10^3 s and in unipolar mode > 10^6 s were recorded. We show how the unique dual-mode switching behavior is enabled by the defect rich polycrystalline material structure of the TiO_2 shell and the interaction between the Ag core and the

Ag electrodes. These results provide a foundation for engineering nonpolar resistive switching behaviors for memory storage and neuromorphic applications in core-shell nanowire structures.

INTRODUCTION:

The study of one-dimensional (1D) nanostructures, such as nanotubes, nanoribbons and nanowires (NWs) has generated promising new technologies, and alternatives to conventional materials due to their unique physical and chemical behaviors, which vary from their bulk and thin-film analogs.[1] Silver (Ag) based nanomaterials have attracted considerable interest with Ag nanowires (AgNWs) being employed in applications such as flexible transparent conductors, thin-film heaters, and photovoltaics.[2-6] There is also considerable interest in the use of nanomaterials for nonvolatile memory technology, where the switching action is controlled by the properties of both the electrodes and the dielectric materials that comprise these devices.[7] Ag for example, is commonly used as an active element in many redox based ReRAM (resistive random access memory) cells. On the other hand, titanium dioxide (TiO_2) is widely used as a dielectric in ReRAM devices. As a material TiO_2 has shown promise in the areas of photocatalysis, water treatment, solar energy conversion, as well as in RS and memristive memory.[8-15] In cation-based ReRAM, bipolar resistive switching (BRS) devices, a low-resistance state (LRS) is established through the formation of a nanoscale metallic conductive filament (CF) from an active electrode (typically Ag or Cu) through an insulator matrix. The CF is dissolved by applying a voltage of the opposite polarity, returning the cell to a high-resistance state (HRS).[16] These devices have low-power consumption, excellent scalability, can display ultra-fast resistive switching (RS) and have strong potential for fabricating multi-state memories.[17-19]

Unipolar resistive switching (URS) involves the formation of CFs through an insulating material which is stable when the voltage bias is removed or inverted. Under larger current application,

increased Joule heating causes the dissolution of this connection. Due to the large currents needed to RESET the device, the power requirements for URS are much higher, and write-endurance lifetimes much shorter when compared to BRS.[20-21]

In this paper, we describe the unique electrical properties that emerge by combining the two materials into a core (Ag) shell (TiO_2) NW structure, denoted as Ag@TiO_2 NWs. Ag@TiO_2 NWs have already been explored as stable and recyclable surface enhanced Raman spectroscopy substrates and efficient photocatalytic materials,[22-23] but to date, the electrical behaviors of Ag@TiO_2 NWs have not been described. Typical ReRAM cells are constructed as planar thin-film metal-insulator-metal (MIM) stacks using a top-down approach and have displayed a wealth of RS behaviors including the co-existence of both URS and BRS.[14, 24-29] The bottom-up approach using self-assembled, and engineered nanostructures offer an alternative platform to investigate the RS phenomenon.[30] The core-shell (CS) structure allows for the ability to control and engineer the properties of the shell (such as thickness and composition) which serves as the switching medium. The conductive core can act as both an interconnect and ion reservoir for the formation of nano-filaments. The RS characteristics of CSNWs have been investigated in Ni@NiO,[31-32] Cu@CuO_x,[33] Cu@SiO_2,[7] Sn-doped In_2O_3@HfO_2,[34] Au@Ga_2O_3,[35] and at the junction of Si@a-Si NWs and crossing Ag electrodes.[36] Recently, Ag@AgO_x CSNWs were deliberately designed in a nanowire network to augment transparent electrodes with RS functionalities.[37]

The presence of both URS and BRS is termed nonpolar switching.[38] CS and TMO NW devices have also shown one of either BRS or URS behaviors, with arrays of multi-layered NiO/Pt NWs demonstrating nonpolar operation.[39] However, to the best of our knowledge, [21, 30, 32, 40] controllable nonpolar operation of a single NW has not yet been reported. We report here on the unique types of RS behaviors that emerge from coating AgNWs with TiO_2. In our case, AgNWs were coated

with sheaths of TiO_2 of varying crystalline qualities depending on fabrication methods, in this study both polycrystalline and amorphous TiO_2 shells were investigated with both passive (Au) and active (Ag) electrodes. These wires can be synthesized in bulk and are stable in solution. By limiting the current allowed to flow through the device during the SET operation, we demonstrate the ability to tailor the electrical polarity response by controllable nonpolar RS with extremely large HRS/LRS ratios in a single two-terminal CSNW device. Based on the results, we propose a switching mechanism based on filament theory to explain the existence of both BRS and URS behaviors.

Methods:

AgNWs were synthesized following the polyol reduction method described by Korte et al. using polyvinylpyrrolidone (PVP) and ethylene glycol as co-mediators.[41] This approach produced uniform AgNWs with the length of several microns and diameters of 63 ± 10 nm; NWs were washed with acetone and water and dried under vacuum at 60 °C.

For polycrystalline CSNWs ($Ag@TiO_2(P)$), a thioglycolic acid (TGA) mediated process was used.[42] In particular, 5 μL of TGA was added to 2.5 mg PVP capped AgNWs in anhydrous ethanol (8 ml) under stirring. After stirring for 30 min, 20 μL of tetrabutyl titanate (TBT) was added dropwise as a TiO_2 source into the solution under inert N_2 atmosphere. The solution was stirred for another 20 min. The final mixture was transferred into a 20 mL Teflon-lined autoclave for solvothermal treatment at 150 °C for 10 h. The resulting sample was washed three times with water and ethanol and centrifuged at 6000 rpm before being dispersed in IPA. For the synthesis of amorphous CSNWs ($Ag@TiO_2(A)$), a one-step solvothermal growth method reported by Du et al. was used.[8] Transmission electron microscopy (TEM) inspection of the wires revealed the

polycrystalline and amorphous nature of the TiO_2 coatings, with thicknesses of 14.6 ± 1.6 nm and 31 ± 7 nm for polycrystalline and amorphous shells respectively.

Single NWs were contacted by electron beam lithography (EBL) after drop-casting a NW/isopropanol dispersion on a clean Si substrate (1 μm thermal oxide) with optical lithography-defined Ti/Au contact pads (5/25 nm). EBL-deposited electrical contacts of Au-Al (30-130 nm), or Ag-Al (100-100 nm) were deposited by thermal evaporation. Devices were capped by MMA(8.5) EL 9 (MicroChem) methyl methacrylate copolymer resist to protect the devices from reacting with the ambient atmosphere. Electrical measurements were carried out at room temperature using a Keithley 4200-SCS. Imaging via scanning electron microscopy (SEM) and EBL was performed on a Zeiss Supra 40. TEM imaging was performed with a JEOL 2100 operated at 200 kV. Scanning TEM (STEM) and energy dispersive x-ray (EDX) elemental analysis were carried out using a FEI Titan microscope at 300 kV.

Results:

RS devices consisted of a Ag@TiO_2(P) CSNW and two Ag electrical contacts as shown in Figure 1(a). TEM inspection confirmed the CS nature of the wire. Figure 1(b) shows inclusions of Ag in the microstructure of the TiO_2 shell; the inset images display elemental maps of the Ag (yellow) and Ti (red) K-edge signals using energy dispersive x-ray (EDX) analysis recorded during scanning transmission electron microscopy (STEM). Similar inclusions were found in the amorphous TiO_2 shells of the CSNWs synthesized by the one-step solution route. These inclusions are likely the result of Ag ion migration during the solvothermal treatment at elevated temperature (~150 °C) in both synthesis methods, their presence may impact the RS properties of the CSNWs and will be discussed later. HRTEM image of the Ag@TiO_2(P) CSNW is given in Figure 1(c),

the magnified region of the CS interface demonstrates the single crystalline nature of the AgNW and polycrystalline structure of the TiO_2 shell (Figure 1(d)). Fast Fourier transform (FFT) pattern from the shell region confirms the polycrystalline rutile crystal structure of the TiO_2 shell. Additional HRTEM image of Ag@TiO_2(P) and EDX mapping of the inclusions observed in the amorphous shell can be found in the supporting information (Figure S1 and S2).

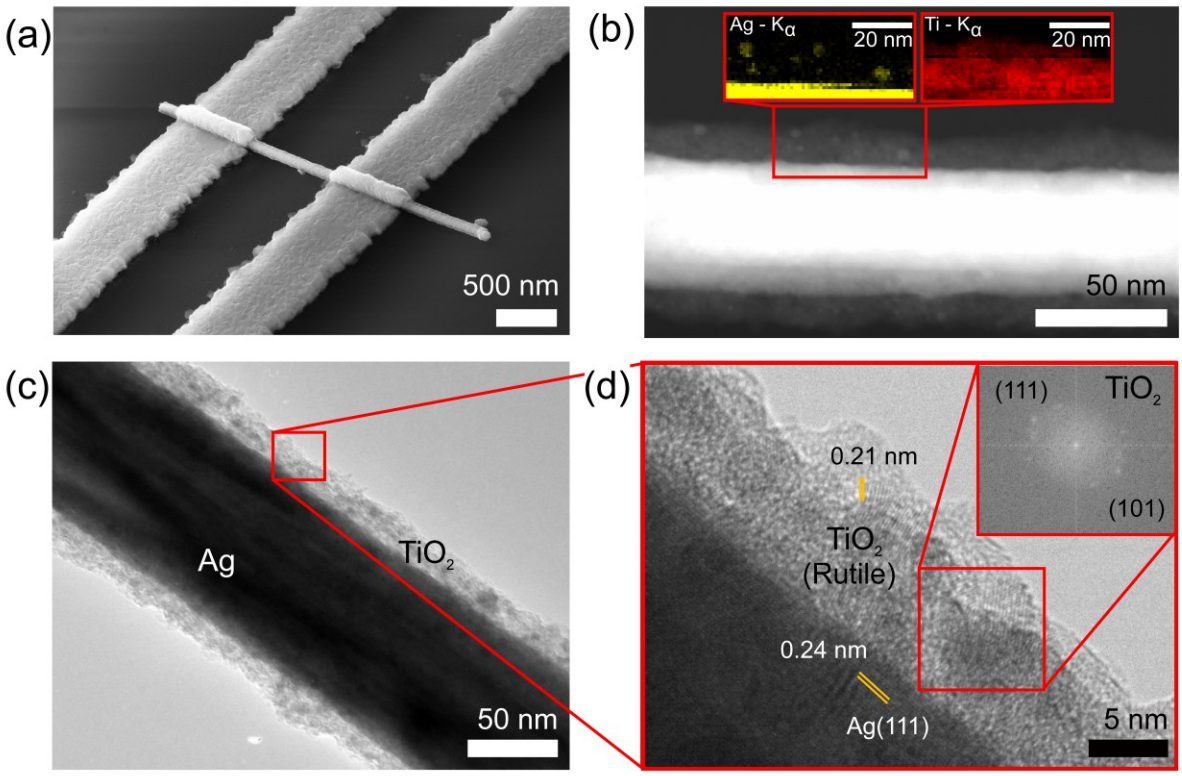

Figure 1. (a) SEM of a two-terminal Ag@TiO_2(P) device contacted with Ag electrodes. (b) STEM image of Ag@TiO_2(P) CSNW, the insets show an EDX area scan on the core/shell interface, inclusions of Ag can be found in the shell as indicated by the Ag (yellow) and Ti (red) K-alpha images. (c) HRTEM image of a Ag@TiO_2(P) CSNW. (d) Magnified area of (c) showing the single crystalline Ag core, and regions of the shell composed of rutile TiO_2, inset is a FFT pattern of the polycrystalline TiO_2 shell.

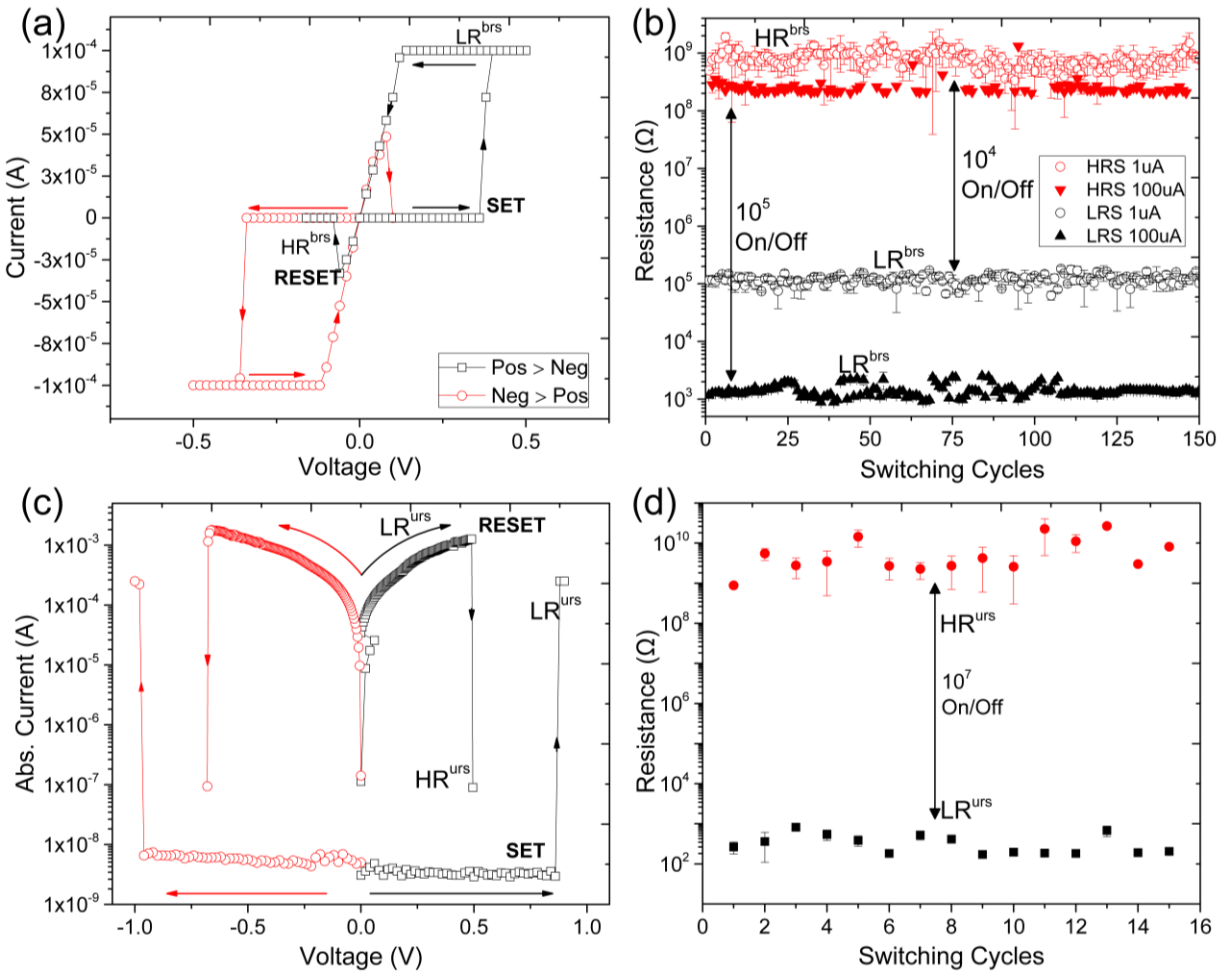

Figure 2. (a) Typical I-V characteristics of the individual Ag@TiO_2(P) CSNW device operating in the bipolar regime SET (from HRS to LRS) to a I_{CC} of 100 μA. (b) HRS and LRS by cycling the forward bias test of (a) multiple times at 1 μA (hollow circle) and 100 μA (shaded triangle) I_{CC}. (c) Typical I-V characteristic in the unipolar regime, I_{CC} for SET was 250 μA, with the I_{CC} being removed for the RESET (from LRS to HRS). (d) Repeating SET and RESET procedures of (c) in the forward bias only. LRS and HRS resistances were read at 0.5 mV.

Figure 2(a) shows typical I-V curves for Ag@TiO_2(P) NWs with Ag electrodes. CSNWs contacted with a pair of Au electrodes displayed only volatile low current switching behavior, known as threshold switching, with electrical failure of the device occurring at currents larger than 1 μA (Figure S3 in the supporting information). As the voltage is swept in the positive direction no current is collected until the device reaches a SET state at 0.4 V. At this value the current jumps six orders of magnitude to the predefined compliance current (I_{CC}) and enters into a bipolar low-resistance state (LR^{BRS}), when the voltage is decreased towards zero the device is ohmic on the return trace with a resistance of 1-2 kΩ. As the voltage continues to be swept with increasing negative bias the current follows linearly until the device experiences a RESET event at -0.1 V and enters the bipolar high-resistance state (HR^{BRS}) with a resistance >100 MΩ. Continuing the sweep in the negative direction causes a second SET event, this can be seen in the red curve of Figure 2(a). The BRS is repeatable over a hundred cycles and displays an ON/OFF ratio of 10^5 as seen in Figure 2(b). By controlling the value of the I_{CC} it is possible to control the LR^{BRS}, at the cost of a reduced ON/OFF ratio (Figure 2(b)). It should be noted that Ag@TiO_2(A) CSNWs contacted with two Ag electrodes failed to demonstrate BRS switching. Ag@TiO_2(A) devices experienced a SET event to a LRS state but were unable to be RESET by the application of a negative bias, a I-V curve showing this behavior is available in the supporting information (Figure S4). The polycrystalline TiO_2 shell offers diffusion pathways which are necessary for the controlled switching in polycrystalline TiO_2; these are not present in the homogeneous amorphous phase TiO_2 CSNWs, this will be discussed later.

The unipolar switching regime for Ag@TiO_2(P) can be accessed by programming a high SET I_{CC} (>150 μA). The URS I-V trace is shown in Figure 2(c), the voltage is increased until a SET event is reached at 0.96 V, at which point the device switches to the unipolar low-resistance state

(LR^{URS}) which is typically ~ 300 Ω. To RESET the device, the I_{CC} is removed, allowing the device to reach high current levels. At a few 100 μAs to mAs the current level suddenly drops to establish the HR^{URS} (which is of a higher resistance than the HR^{BRS}); for the sweep shown in Figure 2(c) the device RESETs at 1.3 mA. Cycling the URS in Figure 2(d) displays an ON/OFF ratio of 10^7. After the device is RESET to the HR^{URS} it may be SET to the LR^{URS} in the opposite voltage direction. By reducing I_{CC} it may also be SET to the LR^{BRS}, this will be demonstrated later in the manuscript. The corresponding amorphous Ag@TiO_2(A) devices could not be RESET, when the I_{CC} was removed and a voltage sweep applied the device presented a typical RESET curve, however, it could not be subsequently SET; SEM imaging revealed that the shell had ruptured and the device had failed (Figure S5).

As mentioned previously, the BRS and URS can be selected by setting the I_{CC} level. To further investigate the transition between switching modes, I-V sweeps with increasing I_{CC} levels were applied until the device transitioned from the BRS to the URS regime. The results of this test are summarized in Figure 3(a), BRS behavior for I_{CC} levels from 50 to 125 μA are presented. At I_{CC} = 150 μA, the device remains in a LRS at negative voltages, consistent with a transition to unipolar behavior. It is also evident that the ON-state resistance of the device is controlled by the magnitude of the I_{CC}, as seen by the change in the slopes of the I-V curve (Figure 3(a)). Through manipulation of the I_{CC}, controllable URS and BRS is demonstrated in Figure 3(b). URS was achieved with a I_{CC} of 200 μA which resulted in a LRS of 200-400 Ω (bottom right inset I-V curve). The LR^{URS} was RESET by removing the current compliance and following the top right inset I-V curve. I_{CC} = 10 μA resulted in repeatable BRS as shown in the middle-inset panel. To determine the effect of the I_{CC} level on the stability of the CF, a sequence of ten (1.7 s) SET pulses were launched into

the device each reaching a predetermined I_{CC} (Figure 3(c)). Each SET pulse was followed by a series of 0.5 mV read pulses to interrogate the evolving resistance of the device.

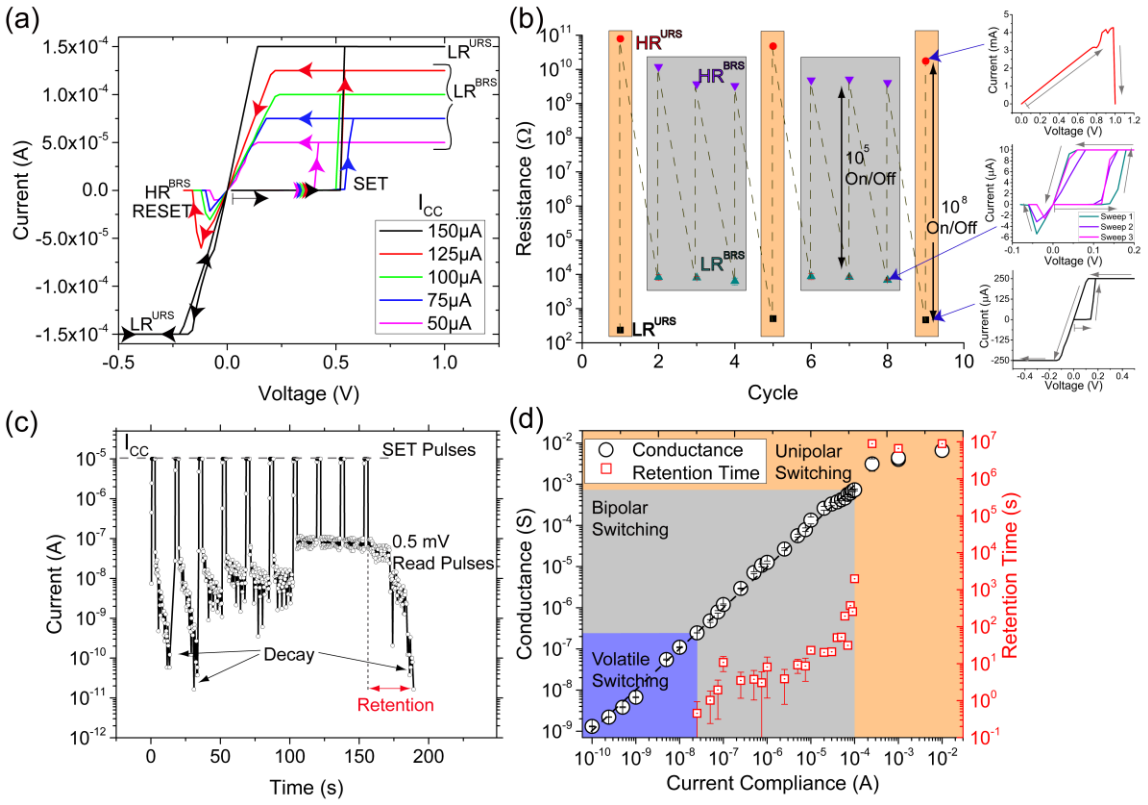

Figure 3. (a) I-V curves of increasing I_{CC} showing the transition from BRS to URS. Up to 125 μA the device RESETs using a negative bias, at 150 μA the device transitions to a URS mode. (b) Controlled operation of URS and BRS by setting a I_{CC} of 200 μA and 10 μA respectively. The inset I-V curves to the right of the main panel show the URS RESET, BRS and URS behavior (top to bottom). (c) I-t curve of ten 1.7 s pulses 15 s apart at I_{CC} = 10 μA, between each SET pulse a (150 ms) 0.5 mV pulse was applied to read the device resistance. (d) Incrementally increasing the I_{CC} in (c) and plotting the retention time and conductance at the SET pulse against the I_{CC} shows the control over the switching regime and corresponding retention time. The dashed line is a linear fit to the volatile and bipolar data. For longer retention times, the conductance of the LR^{URS} was checked each few days, then weeks at 0.5 mV.

After the first 2 SET pulses, the device conductance quickly drops, following the 7th through to the 10th SET pulse the device shows a stable response which continues to be monitored by a 0.5 mV read voltage until it decays. The voltage required to reach and maintain the I_{CC} fell with each pulse, this is illustrated in Figure S6 of the supporting information. The experiment was repeated using a range of I_{CC} levels.

Figure 3(d) displays the dependence of the device conductance with the I_{CC} SET values from 1 nA to 10 mA. The scaling relationship between the LRS and I_{CC} has been previously reported for thin-film programmable metallization cell (PMC) memories.[19, 26, 43-44] A power law relationship is seen to hold for unipolar, bipolar and threshold switching. The blue shaded box in Figure 3(d) highlights the volatile threshold switching regime that occurs at low I_{CC} where the device does not retain the LRS after the voltage is removed and subsequently read, the corresponding memory retention time is zero. At higher I_{CC} the device enters the BRS regime (gray shaded box), where the conductance of the device and the retention time can be set by programming the I_{CC}. The LRS^{BRS} decays over time as previously described, and the rate of decay is controlled by the SET I_{CC}, enabling retention times of seconds, minutes and hours. When the I_{CC} is increased further the device enters the URS regime (orange shaded box), where the conductance level and retention time start to saturate. A number of devices could be SET to I_{CC} of over 1 mA, the retention time of all URS devices was stable for over 10^6 s. Histogram of SET voltages for Ag@TiO_2(P) and (A) can be found in the supporting information (Figure S7).

Many factors were considered in this study to elucidate the RS mechanism, a diagram which illustrates the relationships between the structures, I_{CC}, electrode composition and I-V performances can be found in Figure S8. The role and observation of oxygen vacancies in the RS behaviors of TiO_2 devices have been well documented.[45] Recently dual-filament switching

behaviors have been directly observed in Ta_2O_5-based memristors.[46] However, due to the lack of controllable RS for Au contacted amorphous and polycrystalline CSNWs we do not consider oxygen vacancy species to be a determining factor in the RS mechanism though their presence is expected. Furthermore, a continuous core is critical for current conduction. The Ag electrodes are required to provide a source of ions to mitigate against void formation in the core of the nanowire. These voids appear in CSNWs contacted with Au electrodes (a further discussion and schematic is provided in the supporting information Figure S9).

Based on the experimental evidence of RS in CSNWs contacted with Ag electrodes only, it is most likely that the switching mechanism is dominated by the formation of Ag CFs facilitated by the Ag inclusions and the Ag contacts. A schematic of the SET and RESET behaviors is provided in Figure 4. We propose that under the application of a suitable voltage bias, nanoionic redox processes occur.[21, 26, 19, 47] Ag^+ ions are formed via oxidation at the Ag anode and then migrate through the polycrystalline TiO_2 shell before being reduced at the Ag cathode. The tip of the electrodeposited filament moves back towards the anode as new Ag^+ ions arrive through the lower activation energy pathways found at the grain boundaries of the polycrystalline TiO_2.[26, 48] The growth of this filament is likely to occur in a "winner takes all" scenario, with the favored CF extending out from the cathode bridging the core and contact.[21] The Ag inclusions in the shell are expected to lower the SET voltages by supplying an additional source of cations for the CF. Once a CF bridges the Ag electrode with the Ag core of the wire, the second junction becomes polarized and the CF growth process occurs (Figure 4(a)). The voltages depicted in the schematic only relate to the second CF growth, the transition voltages corresponding to the two-building processes are not shown. Once both junctions are bridged by a CF current flows to reach the I_{CC} and a LRS is established. The formation of the first and then the second junction

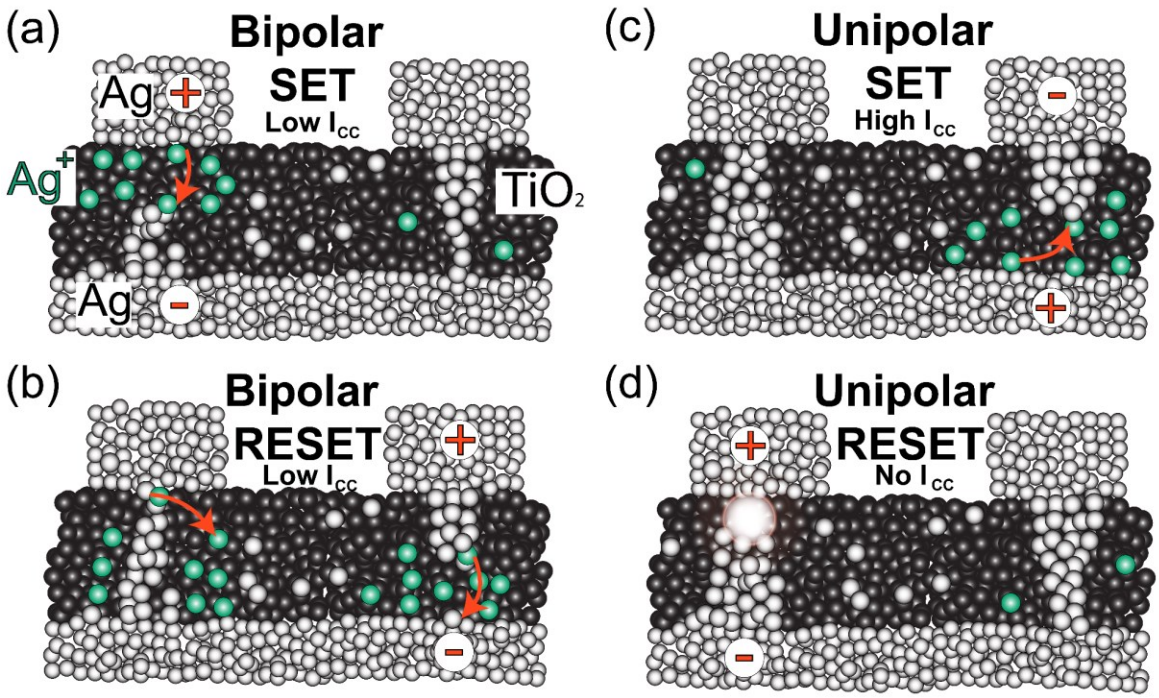

Figure 4. Schematic of SET and RESET conditions in Ag@TiO_2(P) CSNWs. (a) Under low I_{CC} conditions, a bipolar SET is caused by the growth of Ag metallic filaments from the cathode toward the anode due to oxidation and subsequent electrodeposition of Ag^+ ions (shown as the movement of green spheres via red arrows). (b) Under voltage bias inversion, the CF is withdrawn due to the same process. (c) With a higher I_{CC} imposed, a stronger filament can form, which is thicker and more robust than that formed in (a). (d) RESET of the URS due to thermal breakdown (depicted as a radial hot spot) of the CF caused by Joule heating under high current flow with no I_{CC}.

sets an asymmetry in the system which at low I_{CC} allows for the bipolar behavior.

A key factor for the nonpolar operation is setting the device resistance and limiting CF growth by setting the I_{CC}. At very low $I_{CC,}$ an incomplete CF forms which reduces the tunneling gap causing the threshold switching behavior. Increasing the I_{CC} to low levels causes the formation of a bridging CF which is not pronounced enough to be stable to reoxidation and can be dissolved by applying a voltage of the opposite polarity, returning the device to a HRS state (Figure 4(b)). Application of an increasingly negative voltage causes the filaments to regrow, but in the opposite direction as before (not shown schematically) due to the symmetric construction of the device. When a voltage is applied with a high I_{CC}, the CF which physically bridges the Ag electrode and core can supply electrons for subsequent ion reduction allowing the CF to grow radially according to previously developed models.[18] This is expected to result in a conical shape to the CF which is wider at the base and narrows along its length,[21] as depicted in Figure 4(c). It has been previously shown for other Ag CF systems ($Ag/Ge_xS_y/W$ thin-film cells) that the retention time of the ON-state improves as the value of LRS decreases.[49] A feature which is evident from the retention times presented here. The explanation given by several authors align with the proposed mechanism provided in this work, that it results from formation of a thicker, or perhaps growth of multiple metallic filaments which would be slower to erode away.[50]

The URS CF formed at high I_{CC} requires an increased contribution from Joule heating/thermal diffusion to break the connection as illustrated by the thermally dominated hotspot in Figure 4(d). The effect of Joule heating will be greatest at the narrowest part of the bridging CF, which is expected to be at the cathode interface.[21] Experimental evidence presented in this paper shows that polycrystalline TiO_2 CSNWs undergo controllable nonpolar RS sustaining the large currents required for the URS RESET process. Grain boundaries in polycrystalline layers are known to

provide favorable diffusion pathways and enhanced charge transport for migrating species[26, 48, 50-51] which are absent in amorphous layers. This is expected to result in the formation of well-defined, discrete CFs. The same cannot be said for amorphous TiO_2 shelled NWs, where the shell is more homogeneous, and the nanowires ruptured when subjected to large current densities. (See the supporting information for the I-V curve and SEM image (Figure S5)).

It is interesting to contrast our results with similar systems which have been reported in the literature. Ag/TiO_2 combinations have been explored in conventional thin-film two-terminal memory cells, examples of these can be found in TABLE 1. In the work of Hu et al. URS switching was reported with 200 μm^2 Ag contacts and an amorphous 50 nm TiO_2 dielectric spacer. SET voltages of 1 V were observed, with significant SET and RESET currents of 10 mA and 20 mA respectively reported.[29] Using a 100 μm diameter Ag top electrode and an inert Pt bottom electrode, Tsunoda et al. demonstrated BRS in 40 nm polycrystalline/rutile TiO_2 films, with SET voltages of 0.23 V.[26] Similar voltages are required for the RS in this study, the large diameter Ag top electrode and asymmetric nature of the device is expected to result in bipolar operation. Finally, Ghenzi et al. report a device with a polycrystalline anatase TiO_2 layer with millimeter sized contacts showing initial URS behavior which lasts for a hundred cycles then transforms into a BRS only device. While this system demonstrates nonpolar operation, switching between these BRS and URS was not shown to be controllable.[13]

The nonpolar switching observed in our study has some significant advantages over the previously reported thin-film devices given in TABLE 1. It is the only system to show controllable nonpolar operation. Furthermore, it is the first observation of controllable nonpolar operation in a CSNW, the SET and RESET currents observed in Ag@TiO_2(P) are significantly lower than those detailed for the relatively larger thin-film devices. This is attributed to the reduced contact area

over which the applied electric field acts, which in turn leads to a focused CF growth and a reduced number of competing leakage channels. Scaling effects were shown to have a consequence on the unipolar and bipolar behaviors of thin-film devices, as demonstrated in the work of Yanagida et al.[24] CSNWs also require the formation of two junctions, the asymmetry set in the device by formation of one connection and then the other could facilitate the BRS behaviors at low I_{CC} values and URS responses at higher I_{CC} values.

TABLE 1. Two Terminal Thin Film Memory Cells That Have Been Previously Reported, RS Types and ON/OFF Ratios.

author	**memory cell**	**switching type**	**ON/OFF ratio**
Hu et al.[29]	Ag/50 nm TiO_2/Ag	URS	10^2
Tsunoda et al.[26]	Ag/40 nm TiO_2/Pt	BRS	10^8
Ghenzi et al.[13]	Ag/100 nm TiO_2/Si	BRS & URS	10 (BRS) 10^4(URS)
This work.	Ag/30 nm TiO_2/Ag	BRS & URS	10^5(BRS) 10^7(URS)

Conclusions:

In summary, we have investigated the requirements for RS in Ag@TiO_2 CSNW devices. CSNWs were synthesized by two methods resulting in either amorphous or polycrystalline rutile TiO_2 shells surrounding an Ag core. HRTEM and EDX analysis identified the presence of Ag inclusions in the shell of both batches of CSNWs. Neither nanowire system showed controllable RS when contacted with Au electrodes, while dual mode operation of BRS and URS, known as nonpolar RS was observed in CSNWs with polycrystalline TiO_2 coatings contacted with Ag electrodes. The absence of RS in Au contacted Ag@TiO_2(P) demonstrates that the interplay

between the Ag electrodes, Ag inclusions and the Ag core is key to device operation. Operation of BRS and URS could be reversibly selected by defining the I_{CC}, resistance levels differed between URS and BRS modes, allowing them to be readily distinguished, and we postulate the Ag CF associated with the two switching modes are directly related. BRS was demonstrated with over 150 cycles and a tunable retention time up to 10^3 seconds; the conductance of the SET state could also be controlled by programming the pre-defined I_{CC}. ON/OFF ratios were dependent on the I_{CC} as were LRS retention times, ON/OFF ratios and memory retention were found to be highest in URS modes of 10^7 and $>10^6$ s respectively. These findings are significant in the development of CSNW systems and highlight the influence of the shell microstructure material and electrode composition. Moreover, the CSNW system is complimentary to thin film studies, displaying how RS behaviors can be unpredictable as devices are scaled to nm dimensions. Furthermore, it is the first report of controllable nonpolar operation in a single nanowire system; nonpolar operation allows for functional flexibility between short-term and long-term memory which is important for hardware based neuromorphic applications. Future work will include assembly of these CSNWs into nanowire networks, the development of control systems to take advantage of the dual-mode switching and considering other core/shell material combinations to engineer resistive and memristive behaviors.

Supporting Information.

Further information on the amorphous shelled CSNWs, including TEM and STEM analysis, identifying Ag inclusions in the TiO_2 shell. Electrical data such as threshold switching of these wires with Au electrodes and URS SET with Ag electrodes. Electrical data of attempted URS

RESET and subsequent SEM imaging. A diagram considering all experimental variables, and a schematic and discussion related to Au contacted Ag@TiO_2 are also included (PDF).

Corresponding Author

*E-mail: jboland@tcd.ie

Author Contributions.

H.G.M wrote the paper and performed all experiments. S.B synthesized both batches of CS Ag-TiO_2 NWs. J.T.H and J.J.B led the overall effort and co-wrote the paper. All authors discussed and commented on the manuscript and the results.

Conflict of Interest: The authors declare no competing financial interest.

Acknowledgements.

The authors wish to acknowledge funding from the European Research Council under Advanced Grant 321160. This publication has emanated from research supported in part by a research grant from Science Foundation Ireland (SFI) AMBER Centre under Grant Number SFI/12/RC/2278. The facilities and staff at the Advanced Microscopy Laboratory at Trinity College Dublin are acknowledged for their support, in particular, the TEM work performed by Dr Eoin McCarthy.

REFERENCES

1. Hu, J.; Odom, T. W.; Lieber, C. M., Chemistry and physics in one dimension: synthesis and properties of nanowires and nanotubes. *Accounts of chemical research* **1999,** *32* (5), 435-445.
2. Langley, D.; Giusti, G.; Mayousse, C.; Celle, C.; Bellet, D.; Simonato, J.-P., Flexible transparent conductive materials based on silver nanowire networks: a review. *Nanotechnology* **2013,** *24* (45), 452001.
3. Li, B.; Ye, S. R.; Stewart, I. E.; Alvarez, S.; Wiley, B. J., Synthesis and Purification of Silver Nanowires To Make Conducting Films with a Transmittance of 99%. *Nano Letters* **2015,** *15* (10), 6722-6726.
4. Gomes da Rocha, C.; Manning, H. G.; O'Callaghan, C.; Ritter, C.; Bellew, A. T.; Boland, J. J.; Ferreira, M., Ultimate Conductivity Performance in Metallic Nanowire Networks. *Nanoscale* **2015,** *7* (30), 13011-13016.
5. Bellew, A. T.; Manning, H. G.; Gomes da Rocha, C.; Ferreira, M. S.; Boland, J. J., Resistance of Single Ag Nanowire Junctions and Their Role in the Conductivity of Nanowire Networks. *ACS nano* **2015,** *9* (11), 11422-9.
6. O'Callaghan, C.; Gomes da Rocha, C.; Manning, H.; Boland, J. J.; Ferreira, M., Effective medium theory for the conductivity of disordered metallic nanowire networks. *Physical Chemistry Chemical Physics* **2016,** *18* (39), 27564-27571.
7. Catenacci, M. J.; Flowers, P. F.; Cao, C. Y.; Andrews, J. B.; Franklin, A. D.; Wiley, B. J., Fully Printed Memristors from Cu-SiO2 Core-Shell Nanowire Composites. *Journal of Electronic Materials* **2017,** *46* (7), 4596-4603.
8. Du, J.; Zhang, J.; Liu, Z.; Han, B.; Jiang, T.; Huang, Y., Controlled synthesis of Ag/TiO2 core-shell nanowires with smooth and bristled surfaces via a one-step solution route. *Langmuir* **2006,** *22* (3), 1307-1312.
9. Lee, S.-Y.; Park, S.-J., TiO 2 photocatalyst for water treatment applications. *Journal of Industrial and Engineering Chemistry* **2013,** *19* (6), 1761-1769.
10. Wang, G.; Wang, H.; Ling, Y.; Tang, Y.; Yang, X.; Fitzmorris, R. C.; Wang, C.; Zhang, J. Z.; Li, Y., Hydrogen-treated TiO2 nanowire arrays for photoelectrochemical water splitting. *Nano letters* **2011,** *11* (7), 3026-3033.
11. Strukov, D. B.; Snider, G. S.; Stewart, D. R.; Williams, R. S., The missing memristor found. *nature* **2008,** *453* (7191), 80-83.
12. O'Kelly, C.; Fairfield, J. A.; Boland, J. J., A Single Nanoscale Junction with Programmable Multilevel Memory. *ACS Nano* **2014,** *8* (11), 11724-9.
13. Ghenzi, N.; Stoliar, P.; Fuertes, M. C.; Marlasca, F. G.; Levy, P., Resistive switching in Ag–TiO2 contacts. *Physica B: Condensed Matter* **2012,** *407* (16), 3096-3098.
14. Kwon, D.-H.; Kim, K. M.; Jang, J. H.; Jeon, J. M.; Lee, M. H.; Kim, G. H.; Li, X.-S.; Park, G.-S.; Lee, B.; Han, S., Atomic structure of conducting nanofilaments in TiO2 resistive switching memory. *Nature nanotechnology* **2010,** *5* (2), 148-153.
15. O'Kelly, C. J.; Fairfield, J. A.; McCloskey, D.; Manning, H. G.; Donegan, J. F.; Boland, J. J., Associative Enhancement of Time Correlated Response to Heterogeneous Stimuli in a Neuromorphic Nanowire Device. *Advanced Electronic Materials* **2016,** *2* (6).
16. Valov, I., Redox-Based Resistive Switching Memories (ReRAMs): Electrochemical Systems at the Atomic Scale. *ChemElectroChem* **2014,** *1* (1), 26-36.
17. Jameson, J.; Blanchard, P.; Cheng, C.; Dinh, J.; Gallo, A.; Gopalakrishnan, V.; Gopalan, C.; Guichet, B.; Hsu, S.; Kamalanathan, D. In *Conductive-bridge memory (CBRAM) with*

excellent high-temperature retention, Electron Devices Meeting (IEDM), 2013 IEEE International, IEEE: 2013; pp 30.1. 1-30.1. 4.
18. Russo, U.; Kamalanathan, D.; Ielmini, D.; Lacaita, A. L.; Kozicki, M. N., Study of multilevel programming in programmable metallization cell (PMC) memory. *Electron Devices, IEEE Transactions on* **2009,** *56* (5), 1040-1047.
19. Valov, I.; Kozicki, M. N., Cation-based resistance change memory. *Journal of Physics D: Applied Physics* **2013,** *46* (7), 074005.
20. Waser, R.; Aono, M., Nanoionics-based resistive switching memories. *Nature materials* **2007,** *6* (11), 833-840.
21. Ielmini, D.; Waser, R., *Resistive Switching: From Fundamentals of Nanoionic Redox Processes to Memristive Device Applications*. John Wiley & Sons: 2015.
22. Ma, L.; Huang, Y.; Hou, M.; Xie, Z.; Zhang, Z., Ag Nanorods Coated with Ultrathin TiO2 Shells as Stable and Recyclable SERS Substrates. *Scientific reports* **2015,** *5*.
23. Cheng, B.; Le, Y.; Yu, J., Preparation and enhanced photocatalytic activity of Ag@ TiO 2 core–shell nanocomposite nanowires. *Journal of Hazardous materials* **2010,** *177* (1), 971-977.
24. Yanagida, T.; Nagashima, K.; Oka, K.; Kanai, M.; Klamchuen, A.; Park, B. H.; Kawai, T., Scaling effect on unipolar and bipolar resistive switching of metal oxides. *Scientific reports* **2013,** *3*, 1657.
25. Zhu, Y.; Li, M.; Zhou, H.; Hu, Z.; Liu, X.; Fang, X.; Sebo, B.; Fang, G.; Zhao, X., Nonvolatile bipolar resistive switching in an Ag/TiO2/Nb: SrTiO3/In device. *Journal of Physics D: Applied Physics* **2012,** *45* (37), 375303.
26. Tsunoda, K.; Fukuzumi, Y.; Jameson, J.; Wang, Z.; Griffin, P.; Nishi, Y., Bipolar resistive switching in polycrystalline Ti O 2 films. *Applied physics letters* **2007,** *90* (11), 113501.
27. Jeong, D. S.; Schroeder, H.; Waser, R., Coexistence of bipolar and unipolar resistive switching behaviors in a Pt/ TiO2/ Pt stack. *Electrochemical and solid-state letters* **2007,** *10* (8), G51-G53.
28. Kim, K. M.; Kim, G. H.; Song, S. J.; Seok, J. Y.; Lee, M. H.; Yoon, J. H.; Hwang, C. S., Electrically configurable electroforming and bipolar resistive switching in Pt/TiO2/Pt structures. *Nanotechnology* **2010,** *21* (30), 305203.
29. Hu, Y.; Perello, D.; Yun, M.; Kwon, D.-H.; Kim, M., Variation of switching mechanism in TiO 2 thin film resistive random access memory with Ag and graphene electrodes. *Microelectronic Engineering* **2013,** *104*, 42-47.
30. Ielmini, D.; Cagli, C.; Nardi, F.; Zhang, Y., Nanowire-based resistive switching memories: devices, operation and scaling. *Journal of Physics D: Applied Physics* **2013,** *46* (7), 074006.
31. Cagli, C.; Nardi, F.; Harteneck, B.; Tan, Z.; Zhang, Y.; Ielmini, D., Resistive-Switching Crossbar Memory Based on Ni–NiO Core–Shell Nanowires. *Small* **2011,** *7* (20), 2899-2905.
32. He, L.; Liao, Z. M.; Wu, H. C.; Tian, X. X.; Xu, D. S.; Cross, G. L. W.; Duesberg, G. S.; Shvets, I. V.; Yu, D. P., Memory and Threshold Resistance Switching in Ni/NiO Core-Shell Nanowires. *Nano Letters* **2011,** *11* (11), 4601-4606.
33. Liang, K.-D.; Huang, C.-H.; Lai, C.-C.; Huang, J.-S.; Tsai, H.-W.; Wang, Y.-C.; Shih, Y.-C.; Chang, M.-T.; Lo, S.-C.; Chueh, Y.-L., Single CuO x nanowire memristor: forming-free resistive switching behavior. *ACS applied materials & interfaces* **2014,** *6* (19), 16537-16544.
34. Huang, C.-H.; Chang, W.-C.; Huang, J.-S.; Lin, S.-M.; Chueh, Y.-L., Resistive switching of Sn-doped In 2 O 3/HfO 2 core–shell nanowire: geometry architecture engineering for nonvolatile memory. *Nanoscale* **2017**.

35. Hsu, C.-W.; Chou, L.-J., Bipolar resistive switching of single gold-in-Ga2O3 nanowire. *Nano letters* **2012,** *12* (8), 4247-4253.
36. Dong, Y.; Yu, G.; McAlpine, M. C.; Lu, W.; Lieber, C. M., Si/a-Si core/shell nanowires as nonvolatile crossbar switches. *Nano Letters* **2008,** *8* (2), 386-391.
37. Du, H.; Wan, T.; Qu, B.; Cao, F.; Lin, Q.; Chen, N.; Lin, X.; Chu, D., Engineering Silver Nanowire Networks: from Transparent Electrodes to Resistive Switching Devices. *ACS Applied Materials & Interfaces* **2017,** *9* (24), 20762-20770.
38. Akinaga, H.; Shima, H.; Takano, F.; Inoue, I.; Takagi, H., Resistive switching effect in metal/insulator/metal heterostructures and its application for non-volatile memory. *IEEJ Transactions on Electrical and Electronic Engineering* **2007,** *2* (4), 453-457.
39. Huang, Y.-C.; Chen, P.-Y.; Chin, T.-S.; Liu, R.-S.; Huang, C.-Y.; Lai, C.-H., Improvement of resistive switching in NiO-based nanowires by inserting Pt layers. *Applied Physics Letters* **2012,** *101* (15), 153106.
40. Oliver, S. M.; Fairfield, J. A.; Bellew, A. T.; Lee, S.; Champlain, J. G.; Ruppalt, L. B.; Boland, J. J.; Vora, P. M., Quantum point contacts and resistive switching in Ni/NiO nanowire junctions. *Applied Physics Letters* **2016,** *109* (20), 203101.
41. Korte, K. E.; Skrabalak, S. E.; Xia, Y., Rapid synthesis of silver nanowires through a CuCl-or CuCl 2-mediated polyol process. *Journal of Materials Chemistry* **2008,** *18* (4), 437-441.
42. Gale, E., TiO2-based memristors and ReRAM: materials, mechanisms and models (a review). *Semiconductor Science and Technology* **2014,** *29* (10), 104004.
43. Mahalanabis, D.; Barnaby, H.; Gonzalez-Velo, Y.; Kozicki, M.; Vrudhula, S.; Dandamudi, P., Incremental resistance programming of programmable metallization cells for use as electronic synapses. *Solid-State Electronics* **2014,** *100*, 39-44.
44. Tappertzhofen, S.; Valov, I.; Waser, R., Quantum conductance and switching kinetics of AgI-based microcrossbar cells. *Nanotechnology* **2012,** *23* (14), 145703.
45. Jang, M. H.; Agarwal, R.; Nukala, P.; Choi, D.; Johnson, A. C.; Chen, I.-W.; Agarwal, R., Observing Oxygen Vacancy Driven Electroforming in Pt–TiO2–Pt Device via Strong Metal Support Interaction. *Nano letters* **2016,** *16* (4), 2139-2144.
46. Chang, C. F.; Chen, J. Y.; Huang, C. W.; Chiu, C. H.; Lin, T. Y.; Yeh, P. H.; Wu, W. W., Direct Observation of Dual-Filament Switching Behaviors in Ta2O5-Based Memristors. *Small* **2017,** *13* (15).
47. Waser, R.; Dittmann, R.; Staikov, G.; Szot, K., Redox-based resistive switching memories–nanoionic mechanisms, prospects, and challenges. *Advanced materials* **2009,** *21* (25-26), 2632-2663.
48. Mitchell, B. S., *An introduction to materials engineering and science for chemical and materials engineers*. John Wiley & Sons: 2004.
49. Kamalanathan, D.; Russo, U.; Ielmini, D.; Kozicki, M. N., Voltage-driven on–off transition and tradeoff with program and erase current in programmable metallization cell (PMC) memory. *IEEE Electron Device Letters* **2009,** *30* (5), 553-555.
50. Valov, I.; Waser, R.; Jameson, J. R.; Kozicki, M. N., Electrochemical metallization memories—fundamentals, applications, prospects. *Nanotechnology* **2011,** *22* (25), 254003.
51. Lee, M.-J.; Han, S.; Jeon, S. H.; Park, B. H.; Kang, B. S.; Ahn, S.-E.; Kim, K. H.; Lee, C. B.; Kim, C. J.; Yoo, I.-K., Electrical manipulation of nanofilaments in transition-metal oxides for resistance-based memory. *Nano letters* **2009,** *9* (4), 1476-1481.

Supporting Information

Nonpolar Resistive Switching in Ag@TiO_2 Core-Shell Nanowires.

Hugh G. Manning[†, §], *Subhajit Biswas*[§, ϕ], *Justin D. Holmes* [§, ϕ], *John J. Boland* [†, §, *]

[†] School of Chemistry, Trinity College Dublin, Dublin 2, Ireland

[§]Center for Research on Adaptive Nanostructures and Nanodevices (CRANN) & Advanced Materials and Bioengineering Research (AMBER) Research Center, Trinity College Dublin, Dublin 2, Ireland.

[ϕ] School of Chemistry, University College Cork, Cork, Ireland

E-mail: jboland@tcd.ie

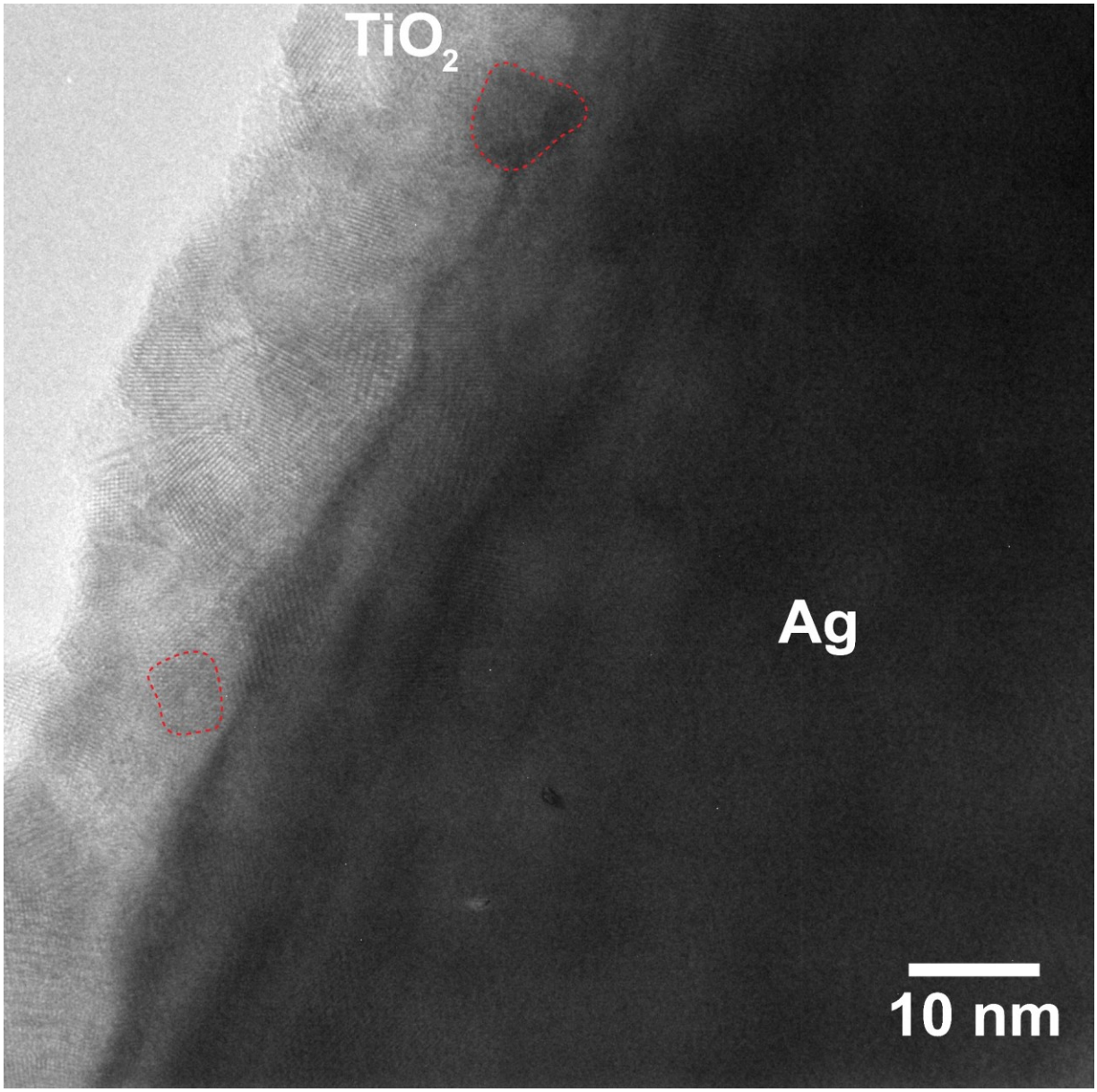

Figure S1. HRTEM image of a Ag@TiO_2(P) CSNW displaying the polycrystalline nature of the TiO_2 shell. Darker regions, such as the two areas highlighted by the dashed red lines indicate inclusions of Ag in the polycrystalline TiO_2 shell.

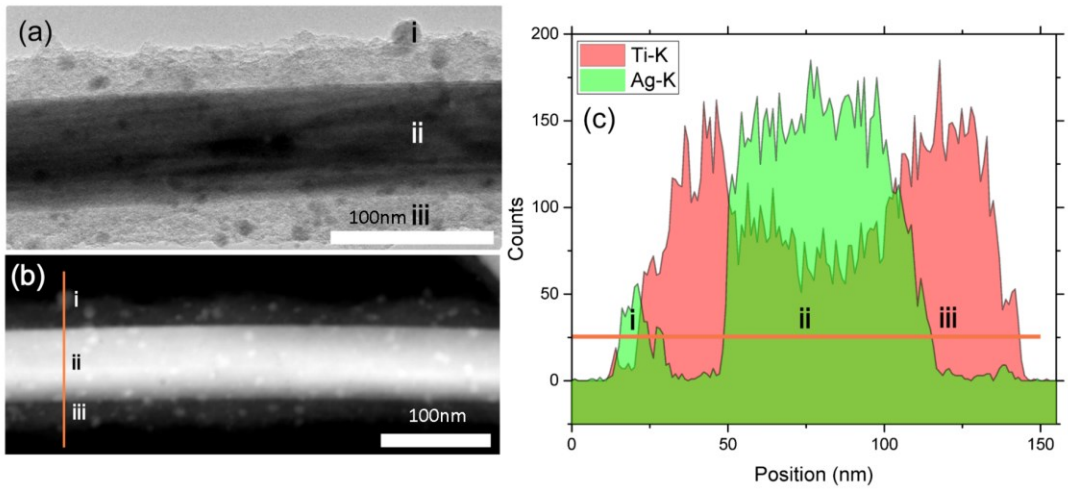

Figure S2. (a) HRTEM of Ag@TiO_2(A) CSNW. (b) STEM image of Ag@TiO_2(A) nanowire, the orange line shows the path of an EDX line scan with three regions: (i) an inclusion in the shell, (ii) the Ag core, and (iii) the TiO_2 shell. (c) EDX line scan confirming the composition of the inclusion and core by the Ag (green) and Ti (red) K-alpha signal.

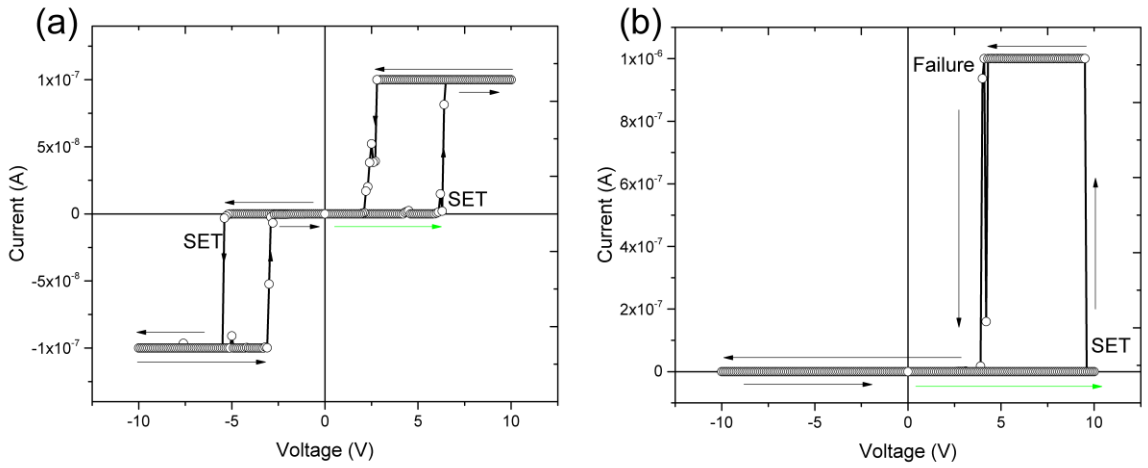

Figure S3. (a) I-V of Au contacted Ag@TiO_2(P) CSNW, SET voltage of 6.5 V to a I_{CC} of 100 nA is much higher than SET voltages for Ag contacted CSNWs. The connection is volatile and cannot be sustained under 2 V. Due to the symmetric construction of the device, the same behavior is observed when sweeping through increasing negative voltages. (b) Failure of the device when the I_{CC} is increased to 1 μA.

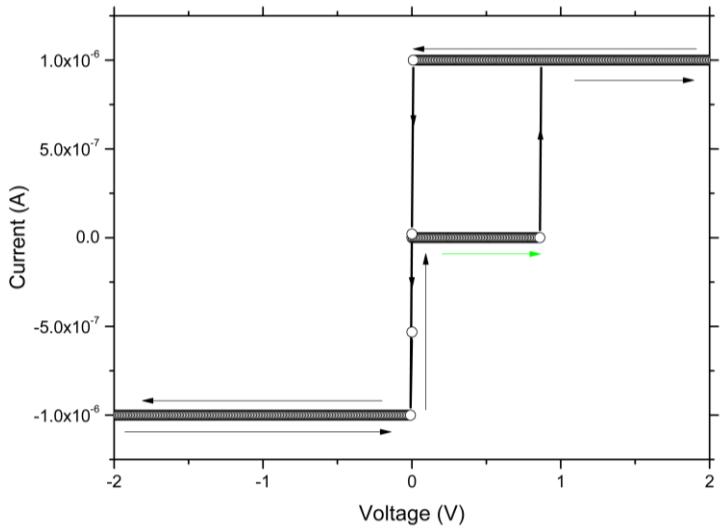

Figure S4. I-V of Ag@TiO_2(A), the device reaches 1 µA I_{CC} at 1 V, and remains in an ON state on the return trace through 0 V and into negative voltages. This demonstrates the lack of BRS.

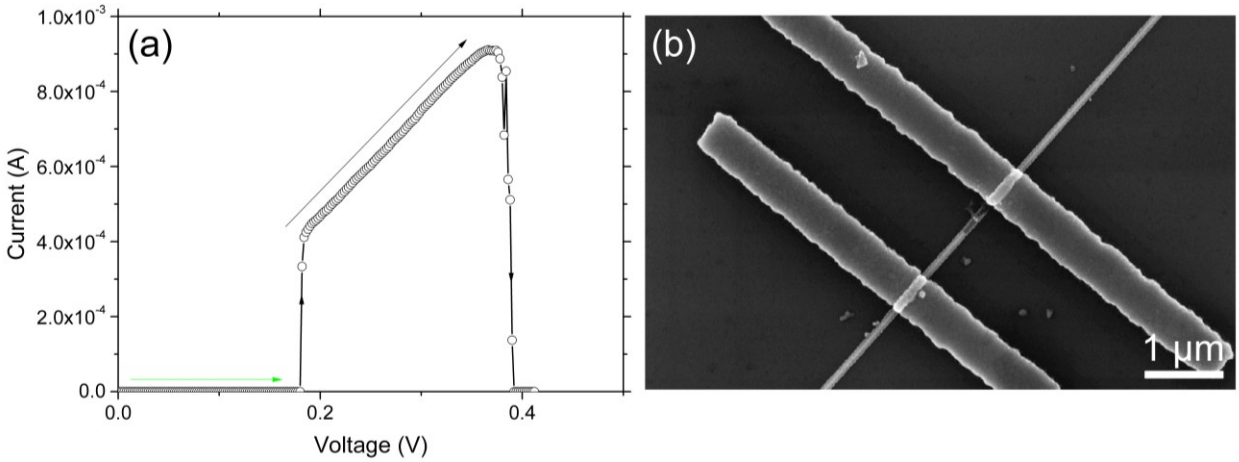

Figure S5. (a) I-V of Ag@TiO_2(A) CSNW with an attempted URS RESET procedure where the I_{CC} was removed and the voltage increased, the current response of the device fails at 900 µA. (b) SEM image of the wire in (a) after the RESET procedure. The CS structure is damaged after the attempted URS RESET.

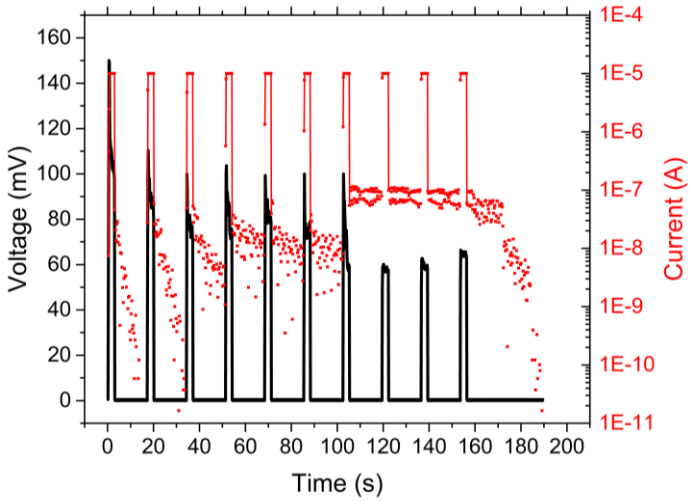

Figure S6. V-t-I curve of ten 1.7 s pulses 15 s apart at I_{CC} = 10 µA, between each SET pulse a (150 ms) 0.5 mV pulse was applied. The current values are plotted in red, the voltage (black trace) required to maintain the 10 µA I_{CC} is shown to gradually decrease.

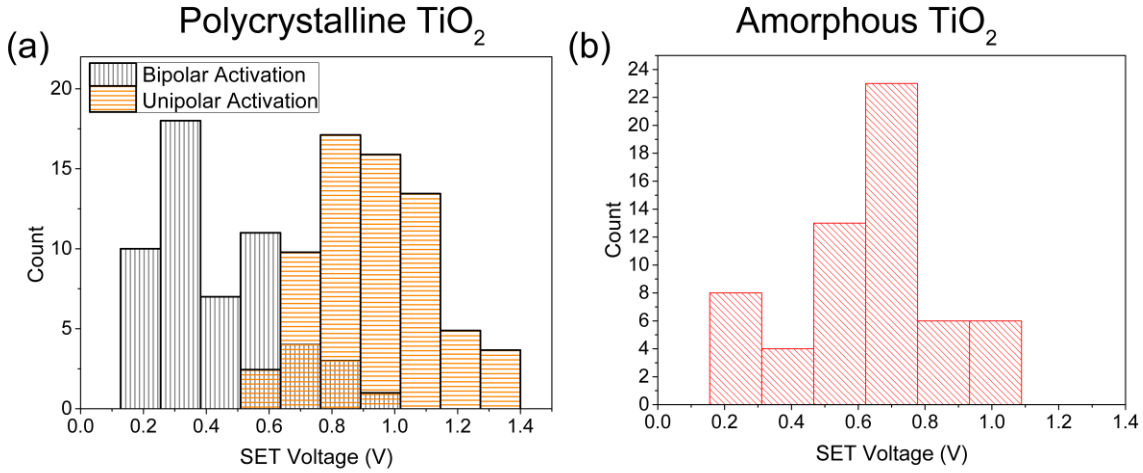

Figure S7. (a) Histogram of voltages required to reach I_{CC} = 100 µA on Ag@TiO_2(P) CSNWS. 100 µA represents the boundary I_{CC} between BRS and URS and so data could be obtained for both regimes. The data compiles 110 switching events across 20 single NW samples. Grey shaded bars show the SET voltages which resulted in BRS, orange cross-hatched bars show the voltages which resulted in URS of the NW. (b) Histogram of SET voltages for I_{CC} = 10 µA on Ag@TiO_2(A) devices.

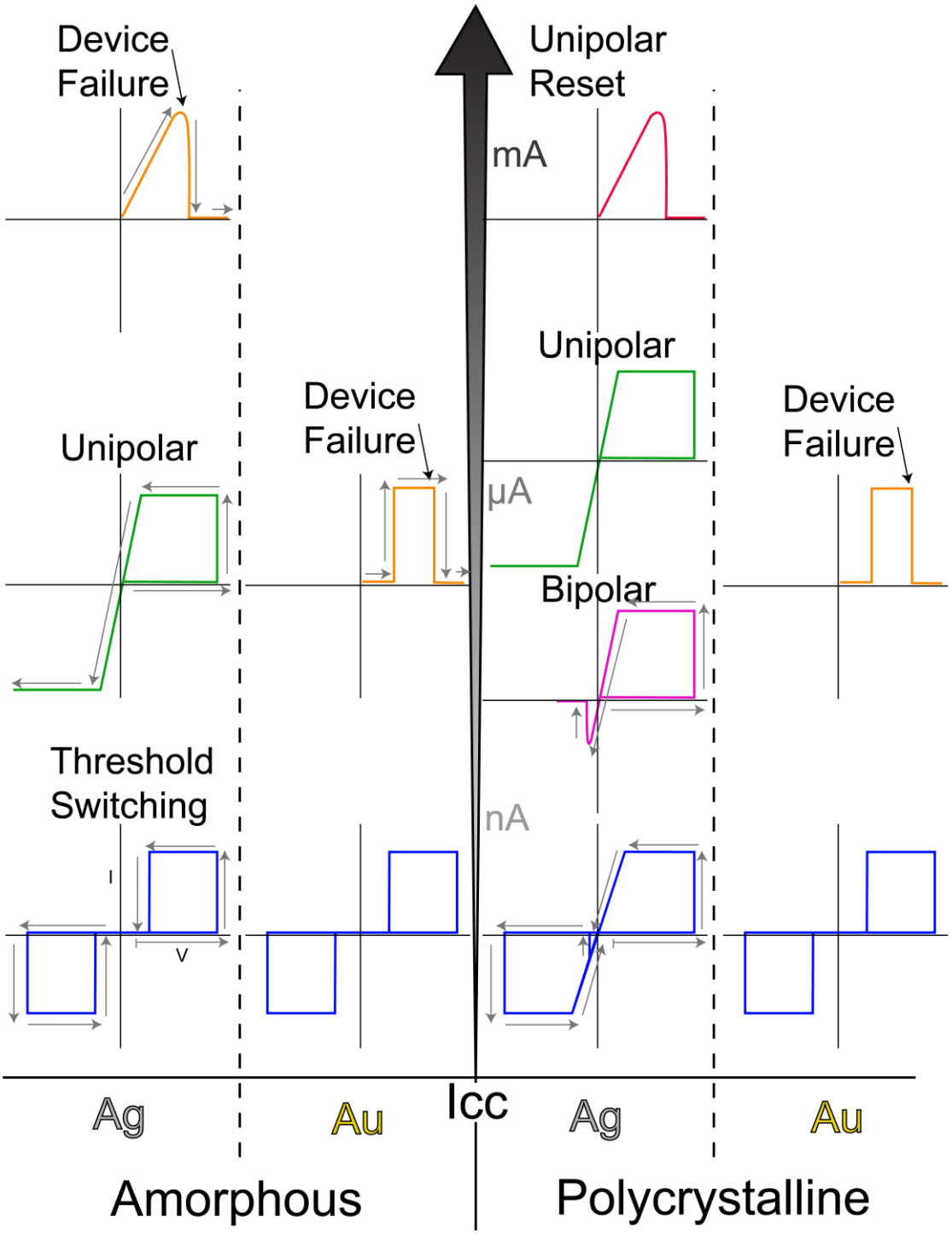

Figure S8. Diagram of the variables involved in the results section of the manuscript. The relationship between amorphous (left) and polycrystalline (right) TiO_2 shell Ag core NWs with respect to increasing I_{CC} (bottom to top), metal contact (Ag left, Au right) and I-V performances are summarized.

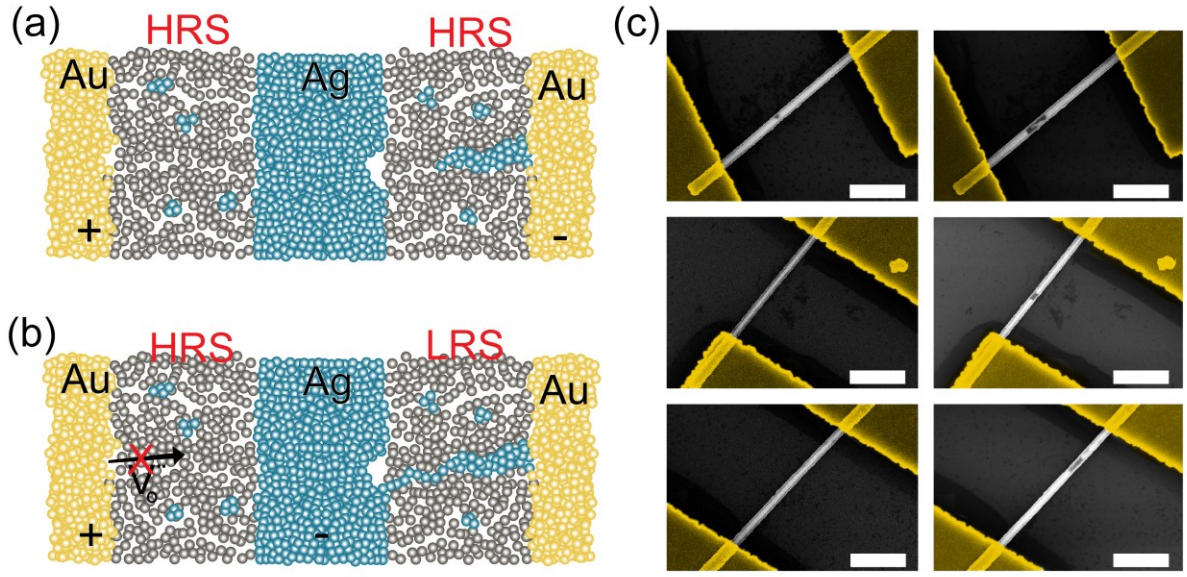

Figure S9. (a) Schematic of Au contacted Ag@TiO_2 CS NWs depicted as a lateral device for illustrative purposes. When a negative bias is applied the Au electrode, redox reactions occur causing the growth of a Ag filament towards the core, the positively charged Au electrode (left) does not attract any Ag^+ species and remains unbridged. (b) As the CF connects the Ag and Au core, the Ag core becomes negatively charged, this should in theory attract positively charged oxygen vacancies from the Au electrode causing a stable LRS. This does not occur (cf. Figure S3), Ag electrodes are required for controllable RS. (c) SEM image of false colored Au contacts to three separate Ag@TiO_2(A) NWs, voids were observed to form in the core of the nanowire indicating the migration of Ag species along the wire and underneath the Ag contact. Scale bars represent 1 μm.

The formation of voids in Au contacted Ag@TiO_2 CSNWs is due to electromigration of Ag species underneath the contact. CSNWs with voids in the core were electrically unresponsive during testing. A continuous core is critical to current conduction and is clearly consumed underneath the electrode when Au contacts are used. Under normal operation conditions using electrodes which are a source of Ag insures a supply to the wire that mitigates against void formation.